International Journal of Recent Technology and Engineering (IJRTE)
ISSN: 2277-3878, Volume-8 Issue-3, September 2019

Effect of Varying Ramp Angle and Leading-Edge Bluntness on the Behavior of Ramp Induced Shock Wave over Triple Ramped Cone Flare Configuration at Hypersonic Speed

Karthik Sundarraj, Ugur Guven, P S Kulkarni, Om Prakash, Ganesh Pawar R

Abstract: ***Numerical simulation results are presented to show the effect of ramp angle variations and leading-edge bluntness on the flow around triple ramped cone flare in hypersonic flow. This study investigates the changes associated with shock wave boundary layer interaction due to ramp induced flow breakdown and the fluctuation in flow in the presence of blunted leading edge. This type of ramp junctions typically features in re-entry vehicles, engine intakes, system and sub-system junctions, control surfaces, etc. Ramp junctions usually are associated with strong separation bubble that has significant upstream influence impacting the effectiveness of aerodynamic surfaces, engine performance, thermal behavior and stability. Computation studies are carried out using finite volume-based RANS solver, accuracy of second order and considering compressible laminar flow characteristics, with solver settings provided similar to experimental conditions as per literature. Comprehensive double ramp studies with suggestions on reducing the separation bubble size are invariantly considered in literature, however there has been no study in understanding the inclusion of additional ramps in such flow scenarios, hence efforts are taken to understand the benefits and implications of including a third ramp along with varying bluntness on the bubble size and its upstream intensity.***

Keywords: Hypersonic, Leading edge bluntness, ramp angle, Shock wave and boundary layer interactions

I. INTRODUCTION

The current technological advancements stand at a stage where the gap between space flight and atmospheric flight are closing in through human interventions and are now a dream that can be realized. The advent of hypersonic vehicle has created hope in this closure of gap and hence a lot of research is conducted in this area.

Manuscript published on 30 September 2019
* Correspondence Author
Karthik Sundarraj*, CFD Software Soln., MSC Software Corporation, Bangalore, India. Email: karthik_sundarraj@yahoo.com
Ugur Guven, Department of Aerospace Engineering, UPES, Dehradun, India. Email: uguven@ddn.upes.ac.in
P S Kulkarni, Aerospace Engineering, Indian Institute of Science, Bangalore, India. Email: psk@iisc.ac.in
Om Prakash, Department of Aerospace Engineering, UPES, Dehradun, India. Email: omprakash@ddn.upes.ac.in
Ganesh Pawar R, Aerospace Engineering, Indian Institute of Science, Bangalore, India. Email: ganesh.pawar66@gmail.com

Man's desire to explore deep space led to many space missions and through these the concept of reentry and reentry vehicles were understood. Apart from hypersonic reentry vehicles there are other hypersonic vehicles such as missiles and transport aircrafts in existence or at least in their nascent stages of development. Most of the reentry vehicles enter earth's atmosphere at very high velocities leading to excessive aerodynamic heating [21].
The temperature of the object becomes very high due to the transformation of kinetic energy of the falling object into heat energy. At such situations the design of the spacecraft is of prime importance. Various researchers [1-10] have investigated shock wave boundary layer and interaction physics through design modifications such as blunting, cavitation, ramping, flaring, external attachments such as aero disc or spike etc. to evaluate and understand the importance of these design features and also to measure the dependency on these features. High speed aerodynamics mainly revolves around shocks and shock interactions that change the course of flow field and their behavior. The heat loads and forces are affected due to these alterations. The study along these lines is called shock wave and boundary layer interaction majorly dealing with the interactions between inviscid and viscous regions [3]. These interactions in the flow affect both internal and external flow aerodynamics. Generation of separation bubble, boundary layer separation, increased heating and even turbulent re-attachment could be caused through the presence of SWBLI. Careful attention must be given to the design of space vehicle subsystems such as wing body junction, engine inlet, nozzle etc., which experience such SWBLI [3]. As an outcome of design refinement several flow control techniques have been developed to suppress the effects of SWBLI [2]. Hypersonic flow field around blunted cone flare is a very good example that exhibits SWBLI. This example exhibits major feature of flows around a space vehicle such as detached bow shock ahead of the cone and oblique shock with boundary layer interaction at the cone flare junction [1]. The SWBLI can produce separated flow at the upstream forward-facing corner where the deflection in the form of a ramp/flare is present. The length of separation has implications for control, stability etc., of a hypersonic reentry vehicle [4]. A separation shock wave is generated due to an abrupt change in flow direction in the presence of ramp. The shock interacts with the boundary layer over the wall which experiences adverse pressure gradient.

Flow separation in the presence of such gradients majorly depends on factors associated with flow conditions, geometrical conditions and boundary layer behaviour. The parameter at interest is the angle known as incipient separation angle given by Needham and Stollery [6].

$$M_\infty \theta_{is} = 80\sqrt{\bar{X}_L} \quad (1)$$

Where $\bar{X}_L$ is the viscous interaction parameter at ramp junctions;

$$\bar{X}_L = M_\infty^3 \sqrt{C} \,/\, \sqrt{Re_L}$$
$$\text{where } C = \frac{\mu_w}{\mu_\infty}\frac{T_\infty}{T_w} \quad (2)$$

Boundary layer separation takes place if the incipient separation angle is lesser than deflection angle. Separation occurs at a point ahead of the compression corner, separation leads to compression waves forming a separation shock ahead of the separation region. Separation bubble can be identified by sudden increase in the pressure from nearly constant in the downstream region to a sudden increase in the compression region. The flow reattaches at a point on the ramp surface, the recirculation zone extends between the separation and reattachment point and the distance between these two points is called as length of separation bubble [2]. In case the ramp angle was smaller than the incipient separation angles the flow would have not undergone much deflection as in the previous case and would have followed a laminar boundary layer profile without separation at the ramp [3]. To enhance the performance of Ramp based SWBLI by reducing the intensity of this interaction through delayed separation several control mechanisms are reported to have been employed. A forward-facing blunted leading-edge is used widely as a control mechanism to control the shock interactions. Leading-edge bluntness completely changes the dynamics of the shock and the boundary layer interaction. The primary reason is the presence of a stronger detached bow shock in place of attached oblique shock. This replacement leads to the formation of strong entropy layer and it interacts with the boundary layer. Flow over the object also gets accelerated due to favorable pressure gradient [4]. Hence a high-speed shear flow approaches the ramp which influences the location of separation bubble, bubble size, incipient separation angle and the reattachment point. Based on research the addition of bluntness to the leading edge provides better suppression of shock interaction when compared to the sharp leading edge.

Several researchers have investigated shock wave boundary layer phenomenon through several design modifications as stated in earlier sections. R. Savino and D. Paterna [1] conducted validation studies of flow around blunted cone flare in hypersonic flows. Experimental studies were performed at the Von Karman Institute H3 Mach 6 wind tunnel in laminar flow conditions. This work gives a detailed insight on the importance of grid independent study and the influence of mesh size on wall pressure, heat flux and skin friction parameters. It has also been noted through this study that the accuracy of separation bubble size, its location, the flow separation and reattachment locations are all dependent on the resolution of mesh near the wall and at the ramp junction. Sensitivity of wall pressure and heat flux to small changes in surface temperature has also been studied in this work. It has been with increase in surface temperature, the separation bubble length increases. The authors have also considered thermal conductivity effects by considering different materials properties of the experimental model and validating the same through computational methods. Bibin John and Vinayak Kulkarni [2 – 4] have performed wide range of numerical investigations addressing the ramp induced shock wave boundary layer interactions. Extensive and in-depth details on the effect of various flow and geometric parameters and their correlation with the shock wave boundary layer interaction in hypersonic flows performed through finite volume based computational solver are presented. Importance of Qualitative approach over quantitative measurements to estimate the separation bubble length and upstream influence through skin friction and wall shear has been detailed out, which gives a clear insight on the method of approach to understand separation physics [3]. The study also clearly points out the fact that the incipient separation angle concept work well only for well separated flows. It is found from these investigations that the separation bubble length is clearly dependent on flow and design parameters. Strong correlation between leading edge bluntness on separation bubble length has been identified and presented. It is understood from this investigation the presence of two critical radius of leading-edge bluntness [4]. The initial trend of leading edge bluntness and separation bubble size indicates that the entropy layer is engulfed by the boundary layer attributing to the increase in bubble length, while further increase in leading edge bluntness leads to the inversion of boundary layer physics wherein the boundary layer gets engulfed by high enthalpy layers when the separation bubble lengths starts to decrease monotonically [3, 4]. From the literature studies it is evident that control of separation bubble is critical to minimize the effects of shock wave interactions with space vehicle systems and sub-systems. It can also be noticed that almost every literature investigation addresses only regions with single and double ramp junctions, but there is almost no research finding related to multi-ramp junctions which also gets featured in such hypersonic vehicle component and system designs. Multi-ramp junctions also pose severe design challenges and it is necessary to take conscious efforts while designing space vehicles. While these previous research works provide very good insights on the SWBLI by varying ramp angles, leading edge bluntness, freestream velocity etc., which becomes the core basis of the current work, while the present research work focuses on the study of shock wave and boundary layer interactions with triple ramp configuration, considering the basic understanding of flow physics around single and double ramp configurations. This way it also helps in understanding the effects of having a third ramp on the upstream separation bubble already present at the second ramp junction along with the understanding of how the presence of third ramp overall changes the shock structure and flow.

Computational investigations are carried out to study and understand the behavior of ramp induced shock wave and boundary layer interactions for three ramp configurations, wherein the first two ramps are considered as specified by R. Savino and D. Paterna [1], while the third ramp angles are varied to study the effect of ramp angle variations on the separation bubble length both at the second and third ramp junctions.

Since the studies presented by Bibin John and Vinayak Kulkarni [4] emphasize the strong correlation between leading edge bluntness and the separation bubble size, it becomes a key consideration to test the correlation on triple ramp configuration and to assess if the leading edge bluntness still continues to be an effective technique for separation control and hence the current research work considers leading-edge radius ranging between 0.5 mm to 5 mm along with a sharp leading edge ramp configuration. Simulation tool validation is performed using the base geometry and boundary conditions as provided by R. Savino [1] in their computational and experimental validation studies. Post successful validation, efforts are taken to initially study the effect of adding a third ramp to the base geometry on the shock wave boundary layer interaction, followed by considering the leading-edge radius effects on these parameters in the presence of third ramp. Details on the solution methodology, model and discretization details are presented in the next section. Discussions on the findings of adding a third ramp with and without leading edge bluntness and its implications on the separation bubble is discussed in Section III, followed by conclusions and future works in Section IV.

II. COMPUTATION METHODOLOGY

The numerical investigations are carried out using High Resolution Flow Solver on Unstructured meshes (HiFUN), considering it to be compressible laminar flow solver. Following conservation equations for mass and momentum are considered in the solver algorithm,

$$\frac{\partial \mathbf{U}}{\partial t} + \frac{\partial (f_i + f_v)}{\partial x} + \frac{\partial (g_i + g_v)}{\partial y} = \mathbf{0} \tag{3}$$

Where,

$$\mathbf{U} = \begin{bmatrix} \rho \\ \rho u \\ \rho v \\ \rho E \end{bmatrix} \quad f_i = \begin{bmatrix} \rho u \\ \rho u^2 + p \\ \rho uv \\ \rho uH \end{bmatrix} \quad g_i = \begin{bmatrix} \rho v \\ \rho uv \\ \rho v^2 + p \\ \rho vH \end{bmatrix}$$

And,

$$f_v = \begin{bmatrix} 0 \\ \tau_{xx} \\ \tau_{xy} \\ u\tau_{xx} + v\tau_{xy} - q_x \end{bmatrix} \quad g_v = \begin{bmatrix} 0 \\ \tau_{xy} \\ \tau_{yy} \\ u\tau_{xy} + v\tau_{yy} - q_y \end{bmatrix} \tag{4}$$

Here, U is the vector of conserved variables, f_i and g_i are inviscid flux vectors along x and y directions respectively. Also f_v and g_v are viscous flux vectors along x and y respectively,

The expressions for the viscous stress and heat conduction terms are given below:

$$\tau_{xx} = \frac{\mu}{Re_\infty}\left(\frac{4}{3}\frac{\partial u}{\partial x} - \frac{2}{3}\frac{\partial v}{\partial y}\right), \quad \tau_{yy} = \frac{\mu}{Re_\infty}\left(\frac{4}{3}\frac{\partial v}{\partial y} - \frac{2}{3}\frac{\partial u}{\partial x}\right)$$

$$\tau_{xy} = \frac{\mu}{Re_\infty}\left(\frac{\partial u}{\partial y} + \frac{\partial v}{\partial x}\right)$$

$$q_x = \frac{\mu}{M_\infty^2 Pr_\infty Re_\infty (\gamma - 1)}\frac{\partial T}{\partial x}$$

$$q_y = \frac{\mu}{M_\infty^2 Pr_\infty Re_\infty (\gamma - 1)}\frac{\partial T}{\partial y}$$

For the present study, fluid is assumed to be as ideal gas. HLLC flux [11, 12] is adopted for inviscid flux scheme and Green Gauss [13] for viscous flux scheme with a special accuracy of 1. Implicit time integration approach is used for obtaining numerical approximation of the solution, with the relaxation faction of 0.4 and the permissible range of CFL (Courant-Friedrichs-Lewy) [19, 20] number is 0.09 – 1.

$$\frac{\mu}{\mu_{ref}} = \left(\frac{T}{T_{ref}}\right)^{\frac{3}{2}}\left(\frac{T_{ref} + S}{T + T_\infty}\right) \tag{5}$$

Laminar viscosity (μ) is computed by using Sutherland's law [18], where (μ_{ref}) is the reference viscosity ($17.16 \times 10^{-6}\ N\,s/m^2$) of air at a reference temperature (T_{ref}) of ($273.15\ K$), the Sutherland's constant (S) for air is considered as (110.56), while the Prandtl number (Pr) is assumed to be 0.74.

III. NUMERICAL INVESTIGATIONS

The model and boundary conditions considered by R. Savino [1] are initially considered to perform inter-code comparison, grid dependency study and theoretical validation stagnation pressure and post shock temperature. The base model considered for initial validation studies is henceforth referred as double ramp, which is 159.11 mm in total length, with first ramp angle 7.5^0, second ramp angle 10^0 and a leading-edge bluntness of radii 3.5 mm. A third ramp of length 63 mm is attached to the base double ramp model along with the consideration of various leading-edge bluntness, for the current investigation on ramp induced shock wave boundary layer interactions. Model details along with the computation domain and boundary conditions are shown in Fig. 1. The freestream conditions and the details about ramp angles and leading-edge bluntness are mentioned in Table-I. Multi-block structured meshing has been performed to discretise the computation domain. Four different mesh combinations with variations in mesh spacing both in normal and along the body are considered, the detailed of the same is shown in Table-II, a sample grid used throughout this investigation is shown in Fig. 2. Due to availability of multiple computation tools,

inter-code comparison was necessary to ensure the chosen tool is the best to capture the flow physics that involves, laminar high-speed flows with high gradient flow separations along with the formation of shocks. The pressure distribution along the double ramp model [1] was taken as a standard to perform the inter-code comparison. Both the simulation tools were run with the same mesh count and boundary conditions, while different solver settings were tried to ensure the best solver setting specific to the tool has been explored. It is evident from Fig. 3, there is excellent agreement with the experimental

pressure plot, the separation and reattachment points for simulations done with HiFUN, for this reason it has been used for all simulations in this investigation. Through grid independence study it was found that the mesh parameters used by R. Savino [1] was not suitable for HiFUN to match the experimental data. Grid spacing normal to the model was found as the major criterion to reach solver

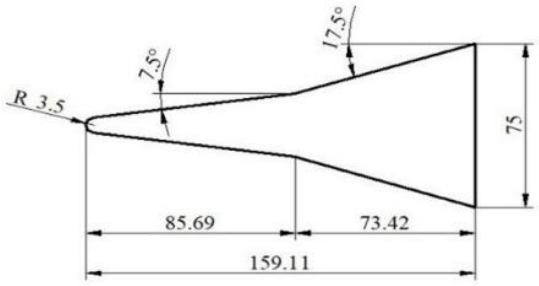

(a) Double Ramp [1]

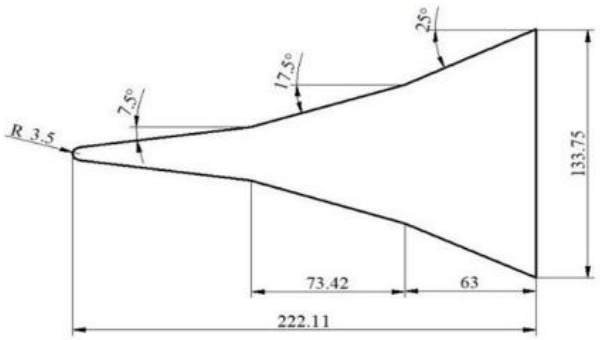

(b) Triple Ramp

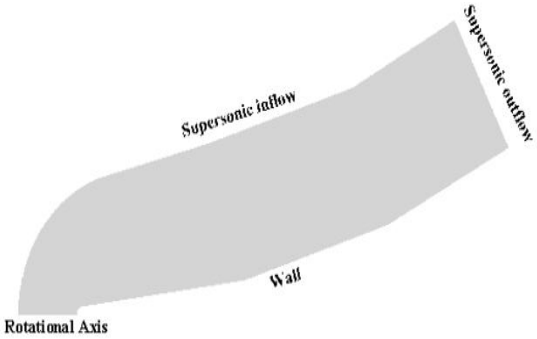

(c) Computational Domain

Fig. 1. Models and computation domain (model dimensions are in mm)

Table-1: Freestream and Geometry Conditions

M_∞	P_∞ (Pa)	T_∞ (K)	μ (Pa-s)	k (N/s-K)	Ramp Angle (α)	Nose Radius (mm)
6	673.67	67.07	$4.47e^{-6}$	0.00607	7.5, 10, 12.5, 15	0, 0.5, 1, 1.5, 2.5, 3.5, 5

Table-II: Details of grids used for grid independence study

Grid	Δn_0	Δn_h	Δs_0	Δs_h
240 x 40 [1]	0.003	0.05	0.0675	0.018
480 x 80 [1]	0.0015	0.005	0.0337	0.009
960 x 160 [1]	0.00075	0.0025	0.0168	0.0045
240 x 40	0.0015	0.0015	0.0675	0.018
480 x 80	0.0015	0.0015	0.0337	0.009
240 x 40	0.015	0.015	0.0675	0.018
480 x 80			0.0337	0.009
660 x 120			0.0337	0.009
960 x 160			0.0168	0.0045
240 x 40	0.03	0.03	0.0675	0.018
480 x 80			0.0337	0.009
660 x 120			0.0337	0.009
960 x 160			0.0168	0.0045
240 x 40	0.045	0.045	0.0675	0.018
480 x 80			0.0337	0.009
660 x 120			0.0337	0.009
960 x 160			0.0168	0.0045
240 x 40	0.06	0.06	0.0675	0.018
480 x 80			0.0337	0.009
960 x 160			0.0168	0.0045

Δn_0, Δn_h = normal spacing at stagnation and ramp; Δs_0, Δs_h= tangential spacing at stagnation and ramp

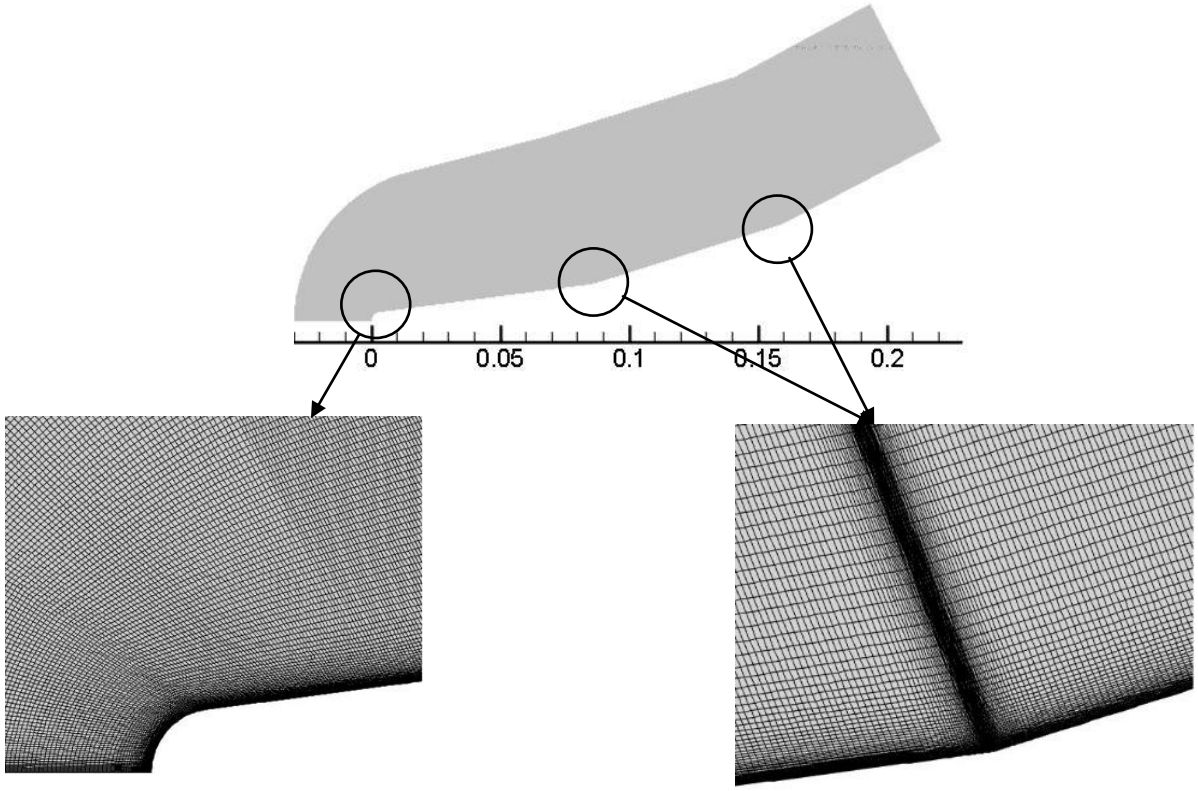

Fig. 2. Sample Grid used for triple ramp

accuracy, while maintaining the overall mesh count same as in literature. It was found from grid independence study that the mesh size of 960 x 160 and 480 x 80 with 30micron normal mesh spacing had excellent agreement with experimental surface pressure values as shown in Fig. 4a. The separation and reattachment points have very good match while there is slight but acceptable computational underprediction in the post attachment zone. It can be noticed that 480 x 80 captures the bubble region better, but the post reattachment region is extremely critical for multi-ramp studies which is captured better by 960 x 160 grid. The importance of qualitative approach to determine the separation bubble length as emphasised by Bibin Jon [3], the skin friction co-efficient parameters were also validated, shown in Fig. 4b. There is underprediction of the separation bubble length as compared to the CFD simulations results in the literature, this could be attributed to the difference in mesh count and the solver setting differences but it is evident that the HiFUN code is predicting the separation bubble length much accurately as indicated in the inter-code comparison. In addition, a theoretical comparison of stagnation pressure and post-shock temperature with simulation outcome using the HiFUN solver also proves the solution to be independent of the grid and the code. Fig. 5a & 5b shows the closer view of stagnation region, where the stagnation pressure value is about 31,683 Pa and the post-shock temperature is 549 K, which matches with values calculated using normal shock theory, where the stagnation pressure is calculated to be 31,538 Pa and temperature 533 K. Similar methodology was followed to perform grid independence study for triple ramp configuration. From the double ramp validation, it was found that 960 x 160 was the most reliable mesh for all design variations and hence the same mesh sizing was continued for triple ramp by adding an equal mesh division on the third ramp making the total mesh size for triple ramp as 1320 x 160, a sample grid independence plot shown in Fig. 6. It is evident that lesser grid size is unable to capture the separation bubble accurately.

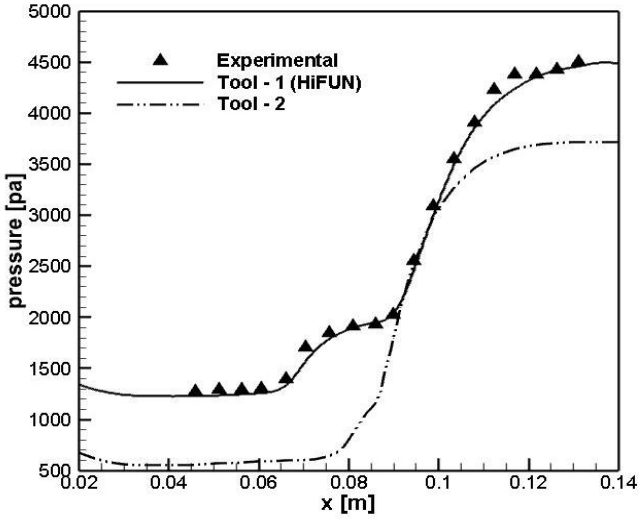

Fig. 3. Inter-code comparison of surface pressure

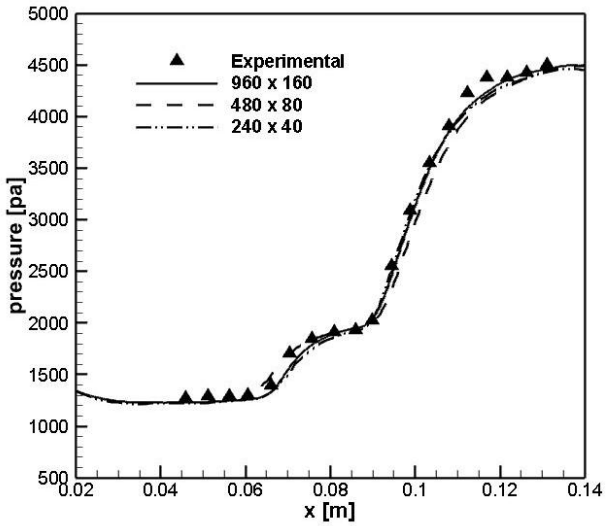

Fig. 4a. Grid independence study of surface pressure profile over double ramp

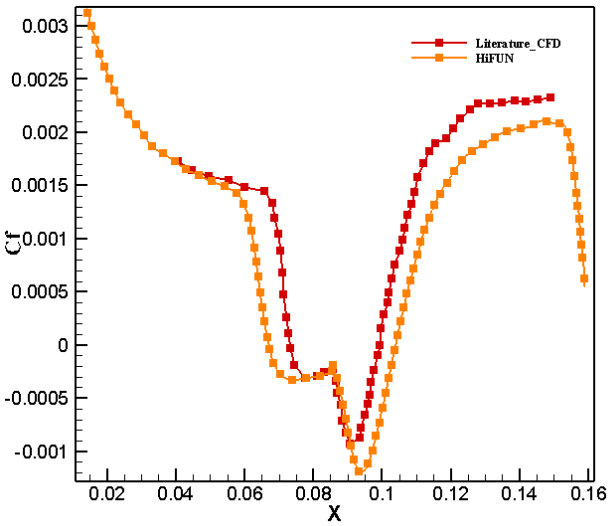

Fig. 4b. Grid independence study of skin friction coefficient

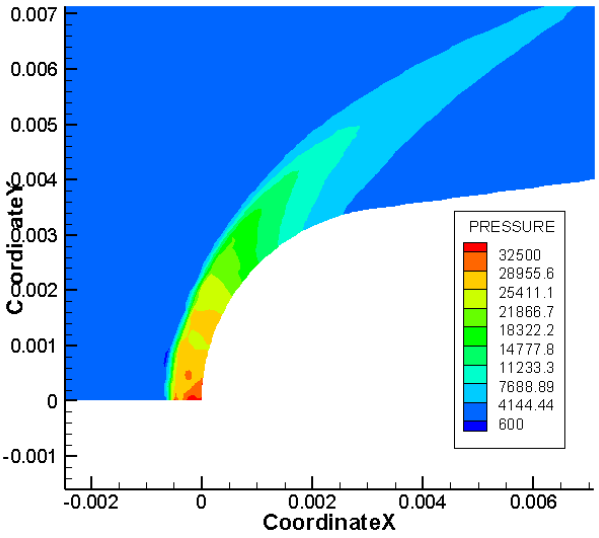

Fig. 5a. Stagnation pressure

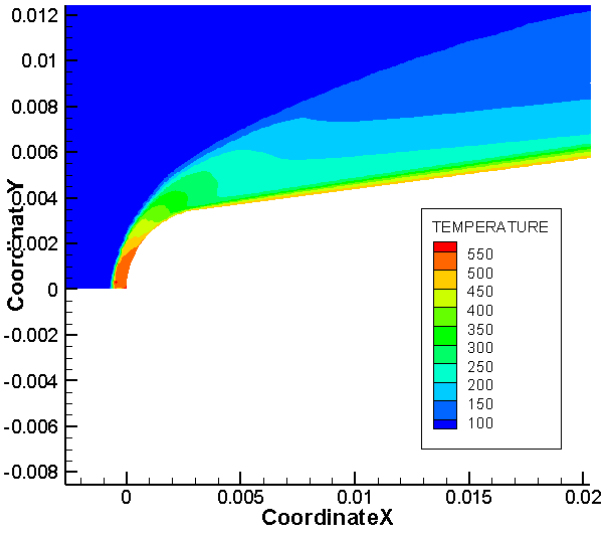

Fig 5b. Stagnation Temperature

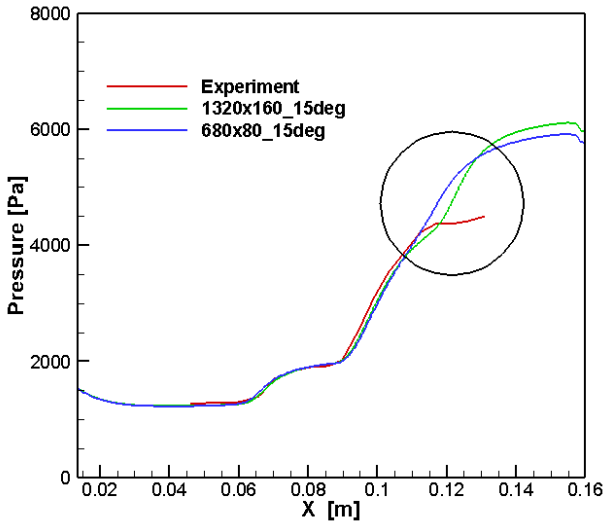

Fig. 6. Grid Independence study of surface pressure over triple ramp

A. Effect of varying ramp angle

The study on effect of adding a third ramp to the standard double ramp model used by R. Savino [1] and consequently varying the third ramp angle are carried out and the changes observed in shock wave boundary layer interactions, separation bubble lengths and surface pressure due to this addition are discussed in this section. This study also enumerates the observations done by Bibin John [3, 4] from the computational studies the importance of reducing the separation bubble length for better design performance and to verify the incipient separation condition through boundary layer separation. The triple ramp configuration (Fig. 1-b) with different third ramp angle $\theta = 7.5^0$, 10^0, 12.5^0 and 15^0 are considered to study the effects of such unique junction configurations. The freestream conditions are as mentioned in Table-1, which are same as per the experiments conducted by R. Savino et al [1].

As mentioned in earlier section the simulation tool has been validated and the grid fixed based on grid independence study done using the experimental data

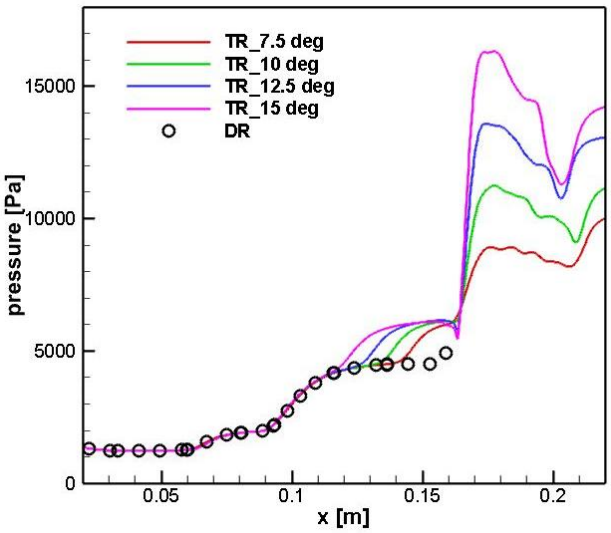

Fig. 7. Effect of third ramp angle variations on pressure distribution

Fig. 8. Effect of third ramp angle on skin friction distribution and bubble length

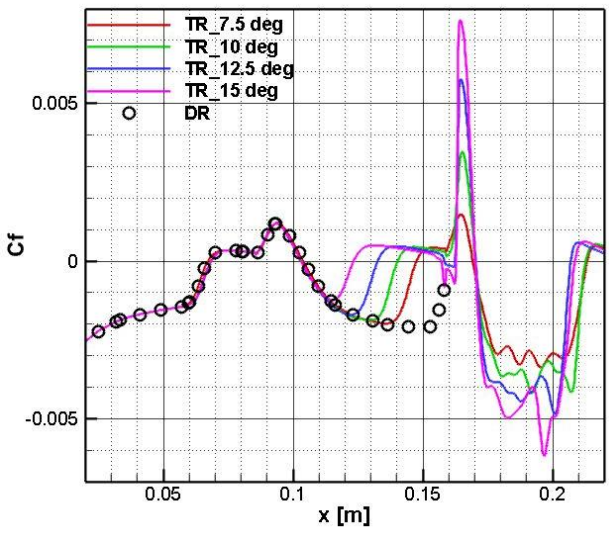

Table-III: Summary on changes in separation bubble parameters

	Double Ramp	Triple Ramp 7.5^0		Triple Ramp 10^0		Triple Ramp 12.5^0		Triple Ramp 15^0	
	FB	FB	SB	FB	SB	FB	SB	FB	SB
L_b	0.0368	0.0366	0.0216	0.035	0.0299	0.0346	0.0378	0.0345	0.0469

L_b = bubble length (in meter), FB = Bubble at 1st ramp junction, SB = bubble at 2nd ramp junction

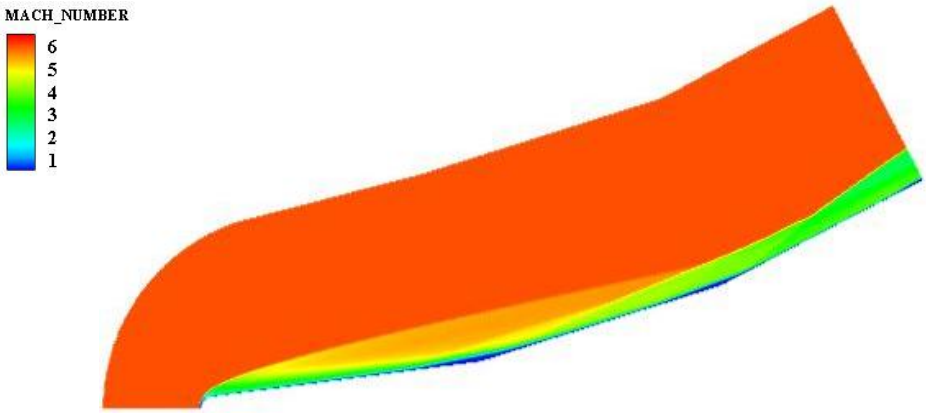

Fig. 9. Shock wave boundary layer interaction over triple ramp configuration (Mach contour)

obtained by R. Savino et al [1], the same grid parameters considered for this study. The variation of surface pressure distribution for different third ramp angles and its implications on the bubble is shown in Fig. 7. The pressure distribution on double ramp is also integrated in the plot to give a perspective on separation bubble of double ramp and the formation of secondary bubble region in case of third ramp. From the graph it can be deduced that the presence of third ramp does not majorly affect the flow over second ramp and follows almost the same pressure trends. As per the findings by Bibin John et al. [3] and Marini [16, 17], the size of separation bubble increases with increase in ramp angle, which continues to be true even with a third ramp as can be seen in the figure. As can be seen in Fig. 9, this configuration has highly complex flow structure, with a detached bow shock at the leading edge, the separation shock at the first ramp along with the reattachment shock forming the first corner shock, which can also be seen in Fig. 7 as a spike in pressure, followed by second corner shock formed due to the second separation bubble, leading to a highly turbulent reattachment shock.

From the pressure distribution plot there is no conclusive evidence on the effects of having a third ramp on the bubble size and based on studies done by Bibin John et al. [4], a quantitative approach is considered by measuring the separation bubble size through skin friction distribution as shown in Fig. 8. The separation and reattachment points are determined where the curves cross the zero line. Summary on the separation bubble details are given in Table-III, where it can be noticed the length of the bubble at the first ramp is decreasing in the presence of a third ramp when compared with the double ramp. These reductions may be small in magnitude but cannot be neglected as the overall objective is to reduce the bubble size and can provide considerable insights for design consideration. Referring to Fig. 8, a clear separation bubble is indicated for ramp angles 7.5^0 and 10^0, while a complex bubble activity can be noticed for 12.5^0 and 15^0 ramp angles. This could be indicative of the presence of a strong and a weak circulation zone caused due to turbulent reattachment or even transitional in the presence of a strong shock which can be noticed in the form a high fluctuation, both in pressure and skin friction plots. It is evident from this simulation study that design considerations while encountering scenarios of ramp type junctions with more than the typical two ramps must be carefully assessed and fine-tuned to ensure reduced flow separations and shock interactions.

B. Effect of blunted leading edge

This study presents a detailed understanding on the effect of blunted leading edge over shock wave boundary layer interactions with triple ramp configuration. The boundary conditions are the same as mentioned in Table-I, with variations in the leading-edge bluntness and ramp angle. The first two ramps are retained as per the experimental model considered by R. Savino et al. [1], while the third ramp with varying angle is attached to this base model. Considering leading edge bluntness is primarily logical as it is nearly impossible to manufacture with a sharp leading edge. Apart from this very point, leading-edge bluntness has significant effect on shock wave and boundary layer, primarily because the bluntness causes a detached bow shock when compared to sharp leading edge with attached oblique shock [3]. Presence of a bow shock reduces the flow velocity approaching the ramp even while the freestream Mach number in both cases are same. Investigations by Bibin John et al. [3] also indicates with reduction in Mach number the shock wave boundary layer integration becomes prominent. Presence of leading-edge bluntness also helps in significantly reducing the surface heating rate and stabilizes the flow through strong circulations at the boundary layer. The computed surface pressure distributions over triple ramp models with varying ramp angles and leading-edge bluntness are shown in Fig. 10 – 13. Commonly noticeable trends in all these surface pressure distribution plots are the behavior of the separation bubble, the reattachment shock and the shear layer region. Interestingly, the length of separation bubble at the double ramp junction is more prominent at lower triple ramp angles (Fig. 10), while the separation bubble at triple ramp junction becomes more prominent at higher triple ramp angles (Fig. 12, 13). This is primarily because the reattachment shock at the double ramp junction tends to grow weaker with combined increment of nose bluntness and the third ramp angle, leading to an early upstream separation at the third ramp junction. What can also be noticed from the pressure distribution plots is that, the reattachment shocks after the double ramp junction is strong but not turbulent over the second ramp, causing a laminar shear region, whereas the reattachment shocks post the triple ramp junction is increasingly strong with increase in third ramp angle and highly turbulent causing a highly unstable shear region over the third ramp. It can be noticed in Fig. 13, there is almost no reattachment at the double ramp junction for both 3.5 and 5 mm blunt radius, there is a considerable downstream shift in the reattachment point at the double ramp junction and upstream shift in the separation point at the triple ramp junction leading to singularization of both the bubbles causing detached flow between both the junctions. The flow reattaches only after the third ramp junction characterized by highly turbulent strong post shock shear region.

The present study also considered the qualitative approach to measure the length of separation bubble though skin friction coefficient. As observed by Bibin John et al. [4] a strong correlation exists between the leading-edge bluntness and the separation bubble length. It is noticed from this study that even bluntness has significant effect on the flow field. Bibin John et al. [3] identified the presence of two critical nose radius, inversion and equivalent radius. The separation bubble size increases with increase in blunt radius (BR) until it reaches the inversion radius. This increase in separation bubble size is attributed to the dominance of boundary layer over the entropy layer. Post the inversion radius the bubble tends to decrease in size with increase in leading-edge bluntness due to the shift in dominance of entropy layer over boundary layer. Computational results of skin friction coefficient over triple ramp configuration with varying blunt radius is shown in Fig. 14 – 17. Similar to the pressure distribution plots it is noticed that the separation bubble size at the double ramp decreases in size with increase in third ramp angle and the reverse is noticed with respect to the bubble size at the third ramp junction. In case of 15^0 third ramp angle the separation behavior is reconfirmed through Fig. 17, where it can be noticed that the reattachment does not occur post the double ramp junction leading to detached flow between both the junctions. From the skin friction coefficient, the separation and reattachment points can be located as the ones where the distribution curve crosses the x-axis line. The changes in the locations of these two points for different third ramp angles along with different leading-edge radii are plotted in Fig. 18. Separation and reattachment points of both the separation bubbles, one over double ramp junction called as first bubble (FB) and the other over triple ramp junction called as second bubble (SB) are both considered for analogy in this plot. From this figure it is evident, with initial increase in leading edge blunt radius the separation point shifts upstream and the reattachment point shifts downstream, increasing the separation bubble length for initial radii indicating the dominance of boundary layer over entropy layer.

The first critical radius or the inversion radius is noticed anywhere between 3.8^0 to 4.4^0 where the boundary layer and the entropy layer are assumed to be of same thickness. With further increase in leading-edge radius, the separation point seems to move downstream, and the reattachment point upstream decreasing the length of the separation bubble, indicating the fact the dominance of entropy layer over boundary layer. Yet again it can be noticed the reattachment point for 15^0 third ramp angle is increasing with increase in blunt radius and the separation point also indicating the same proving completely detached flow. It also confirms that the addition of third ramp does not alter the correlation between blunt radius and the separation bubble length as reported by Bibin John et al. [3, 4], while there are noticeable upstream effects on the separation, reattachment and the overall shock wave boundary layer interaction.

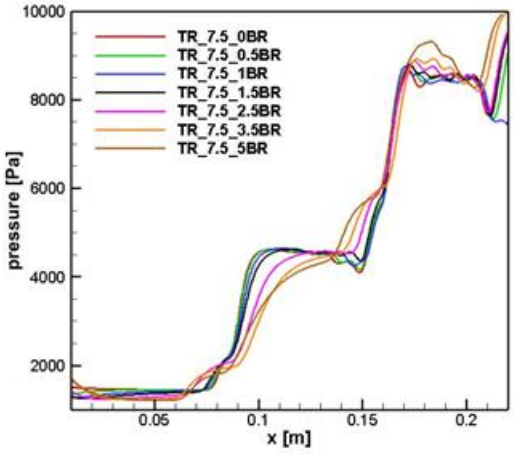

Fig. 10. Pressure distribution over 7.5^0 third ramp angle

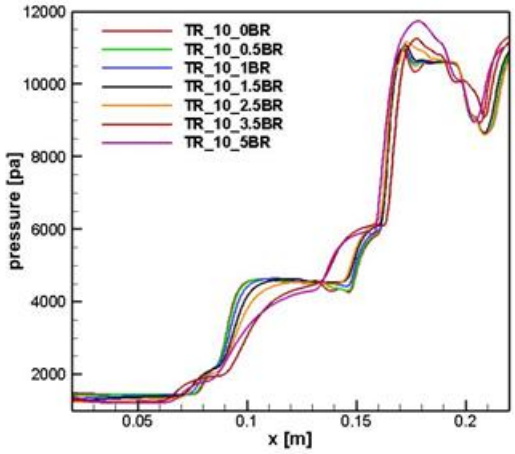

Fig. 11. Pressure distribution over 10^0 third ramp angle

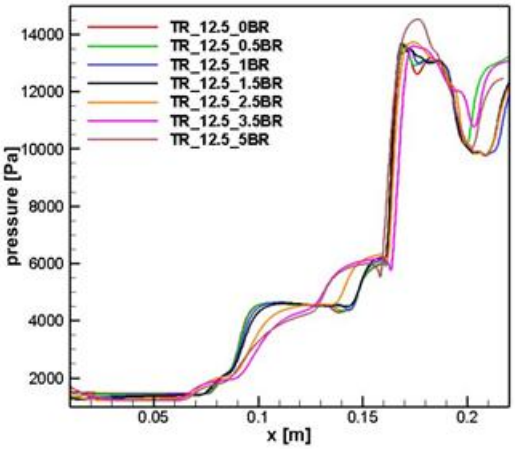

Fig. 12. Pressure distribution over 12.5^0 third ramp

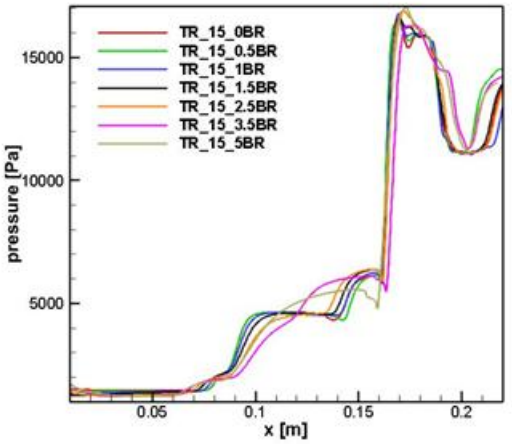

Angle Fig. 13. Pressure distribution over 15^0 third ramp angle

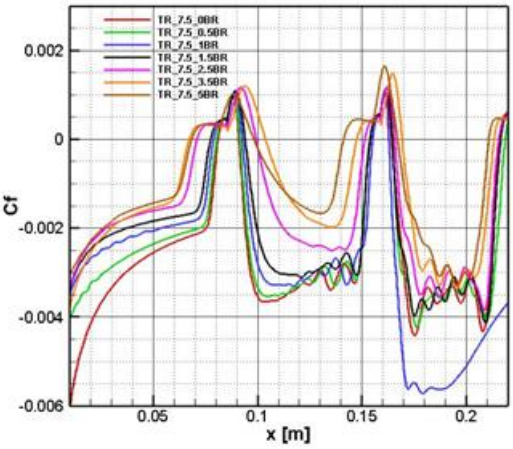

Fig. 14. Skin friction coefficient over 7.5^0 third ramp angle for different leading-edge radius

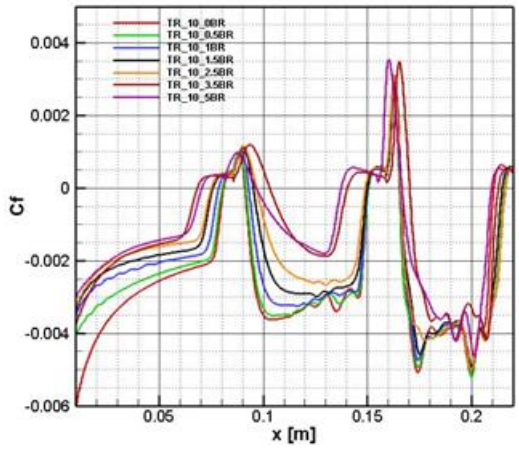

Fig. 15. Skin friction coefficient over 10^0 third ramp angle for different leading-edge radius

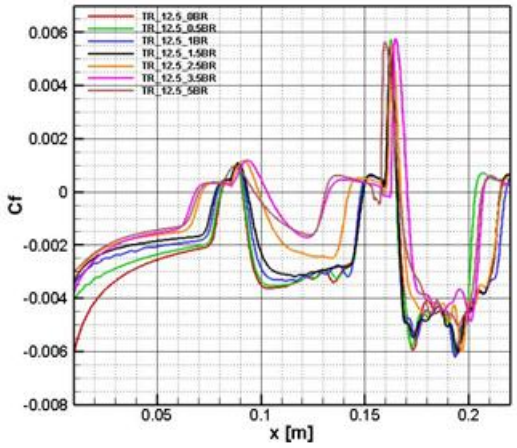

Fig. 16. Skin friction coefficient over 12.5^0 third ramp angle for different leading-edge radius

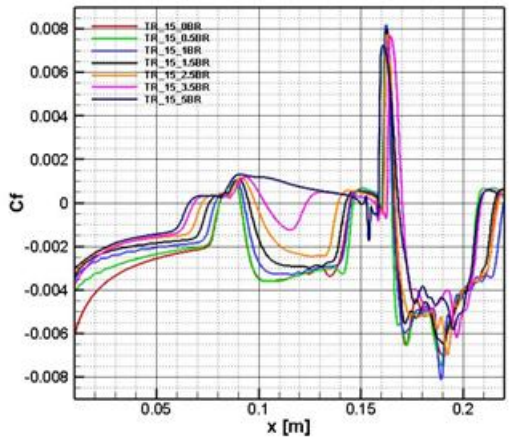

Fig. 17. Skin friction coefficient over 15^0 third ramp angle for different leading-edge radius

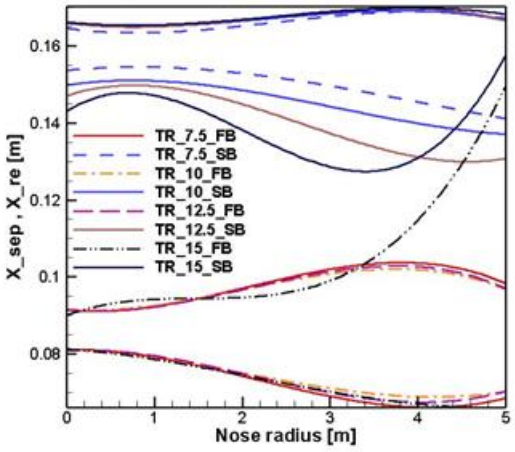

Fig. 18. Separation and reattachment points variation for different blunt radii and third ramp angle

IV. CONCLUSION

Numerical investigations were performed to investigate the effects of varying different geometrical parameters on the shock wave and boundary layer interaction physics in laminar hypersonic flow regime using high resolution flow solver HiFUN. Extensive validation activity was performed to ensure accuracy of flow solver through inter-code comparison and grid independence based on which a common solver and grid was chosen as the outcome of this validation. Efforts were taken to initially study the effect of adding a third ramp on the shock wave and boundary layer interaction, followed by considering the variations in leading-edge radii in combination with varying third ramp angle. This study focused on studying a niche area of multi-ramp configurations, in this case triple ramp configuration which does not feature much in any of the past literatures, but poses equal or even higher design challenges due to the complexity in flow patterns, separation and attachment physics and highly turbulent shear region. Both qualitative and quantitative methods are employed to understand the overall effects of these design configurations on the shock wave boundary layer interaction. From computational studies it is noted that the triple ramp configuration has highly complex flow structure, with a detached bow shock at the leading edge, the separation shock at the first ramp along with the reattachment shock forming the first corner shock, followed by second corner shock formed due to the second separation bubble, leading to a highly turbulent reattachment shock. This proves that computation methods can no more assume laminarity and must consider turbulent flow modeling for upcoming research studies. Quantitative study by measuring the separation bubble size through skin friction distribution indicates the length of separation bubble at the first ramp decreases in the presence of a third ramp when compared with the double ramp. These decrements though small in magnitude cannot be neglected as the overall objective is to reduce the bubble size and can provide considerable insights for design consideration.

The skin friction distribution also shows a clear separation bubble for smaller third ramp angles, while a complex bubble activity can be noticed for higher ramp angles. This could be indicative of the presence of a strong and a weak circulation zone caused due to turbulent reattachment or even transitional in the presence of a strong shock. Study on effect of varying the leading-edge bluntness offered some interesting outcomes wherein, the length of separation bubble at the double ramp junction is more prominent at lower triple ramp angles, while the separation bubble at triple ramp junction becomes more prominent at higher triple ramp angles. It has been identified that the reattachment shock at the double ramp junction tends to grow weaker with combined increment of nose bluntness and the third ramp angle, leading to an early upstream separation at the third ramp junction. What was also noticed from the pressure distribution plots is that, the reattachment shocks after the double ramp junction is strong but not turbulent over the second ramp, causing a laminar shear region, whereas the reattachment shocks post the triple ramp junction is increasingly strong with increase in third ramp angle and highly turbulent causing a highly unstable shear region over the third ramp. The first critical radius or the inversion radius is noticed anywhere between 3.8^0 to 4.4^0, with further increase in radii leading to a reduction in separation bubble size. It is evident that design considerations while encountering scenarios of multi-ramp type junctions must be carefully assessed and fine-tuned to ensure reduced flow separations and improved shock interactions. Future study will explore effects of changes in freestream conditions such as Mach number and surface property changes such as temperature. Additional design changes shall also be considered by adding more ramps to the typical base configuration and ensuring the consideration of turbulence in the flow to better predict the separation bubble dynamics.

V. ACKNOWLEDGEMENT

Authors are thankful to Prof. N Balakrishnan and Dr. Nikhil Shende for their continued support with HiFUN solver and for providing timely guidance. Thanks to Prof. P S Kulkarni for allowing access to his Computation mechanics laboratory to perform all the computational investigations.

REFERENCES

1. R. Savino and D. Peterna, "Blunted cone-flare in hypersonic flow," Computers & Fluids, pp. 859-875, 2005.
2. B. John and V. Kulkarni, "Numerical assessment of correlations for shock wave boundary layer interaction," Computers & Fluids, vol. 90, pp. 42-50, 2014.
3. B. John, V. Kulkarni and G. Natarajan, "Shock wave boundary layer interactions in hypersonic flows," International Journal of Heat and Mass Transfer, vol. 70, pp. 81-90, 2014.
4. B. John and V. Kulkarni, "Effect of leading edge bluntness on the interaction of ramp induced shock wave with laminar boundary layer at hypersonic speed," Computers & Fluids, vol. 96, pp. 177-190, 2014.
5. S. Reichel and R. Groll, "Numerical simulation and experimental validation of a hypersonic flow for numerical modulation of re-entry phenomena prediction using adaptive mesh refinement," International Journal of Computational Methods and Experimental Measurements, vol. 1, no. 4, pp. 381-394, 2013.
6. D. A. Needham and J. L. Stollery, "Boundary layer separation in hypersonic flow," University of London, 1966.
7. C. L. Runninga, T. J. Julianoa, J. S. Jewell, M. P. Borgb and R. L. Kimmel, "Hypersonic Shock-Wave/Boundary-Layer Interactions on a Cone/Flare," Experimental Thermal and Fluid Science, 2019.
8. D. V. Gaitonde, "Progress in shock wave/boundary layer interactions," Progress in Aerospace Sciences, vol. 72, pp. 80-99, 2015.
9. I. G. Brykina, B. V. Rogov, G. A. Tirskiy, V. A. Titarev and S. V. Utyuzhnikov, "A comparative analysis of approaches for investigating hypersonic flow over blunt bodies in a transitional regime," Journal of Applied Mathematics and Mechanics, vol. 77, pp. 9-16, 2013.
10. H. S. Massimi, H. Shen, C. Y. Wen, Y. S. Chen and S. M. Lian, "Numerical analysis of hypersonic flows around blunt-nosed models and a space vehicle," Aerospace Science and Technology, vol. 43, pp. 360-371, 2015.
11. Z. Shena, W. Yan and G. Yuan, "A robust HLLC-type Riemann solver for strong shock," Journal of Computational Physics, vol. 309, pp. 185-206, 2016.
12. S. Simon and M. J. C, "A simple cure for numerical shock instability in the HLLC Riemann solver," Journal of Computational Physics, vol. 378, pp. 477-496, 2019.
13. H. Nishikawa, "From hyperbolic diffusion scheme to gradient method: Implicit Green–Gauss gradients for unstructured grids," Journal of Computational Physics, vol. 372, pp. 126-160, 2018.
14. D. Sun, F. Qu and C. Yan, "An effective flux scheme for hypersonic heating prediction of re-entry vehicles," Computers and Fluids, vol. 176, pp. 109-116, 2018.
15. F. Qu, J. Chen, D. Sun, J. Bai and G. Zuo, "A grid strategy for predicting the space plane's hypersonic aerodynamic heating loads," Aerospace Science and Technology, vol. 86, pp. 659-670, 2019.
16. F. Grasso and M. Marini, "Analysis of hypersonic shock-wave laminar boundary-layer interaction phenomena," Computers & Fluids, vol. 25, no. 6, pp. 561-581, 1996.
17. M. Marini, "Analysis of hypersonic compression ramp laminar flows under sharp leading edge conditions," Aerospace Science and Technology, vol. 5, no. 4, pp. 257-271, 2001.
18. W. Sutherland, "The viscosity of gases and molecular force," Philosophical Magazine Series 5, vol. 36, pp. 507-531, 1893.
19. H. Mahgerefteh, Y. Rykov and G. Denton, "Courant, Friedrichs and Lewy (CFL) impact on numerical convergence of highly transient flows," Chemical Engineering Science, vol. 64, no. 23, pp. 4969-4975, 2009.
20. J. H. Ferziger and M. Peric, Computational Methods for Fluid Dynamics, Delhi: Springer.
21. J. D. Anderson Jr, Hypersonic and High Temperature Gas Dynamics, New Delhi: McGraw Hill, 2011.

AUTHORS PROFILE

Mr. Karthik Sundarraj is an Aerospace Engineer with a Master of science, specialized in CFD from Brunel University, London. He currently works as the Technical Manager handling CFD Solutions portfolio for Indo-Pacific region at MSC Software Corporation. He comes with a rich industrial experience handling multiple CFD and other technology teams. He also worked as a Professor at UPES, Dehradun where he coordinated M.Tech in CFD program. He possesses strong research exposure working majorly in the areas of High-speed flows, external and internal flows. His other areas of interest include CFD applications in Biomedical, automotive and sports sectors. He has been associated with IISc since 2009, started as Project assistant and then moved on to be a research associate and later continued the association through collaborated projects and research initiatives.

Prof. Dr. Ugur Guven is an Aerospace Engineer (PhD, BSc) and a Nuclear Engineer (MSc). He is of now currently working as the Senior Professor of Aerospace Engineering at UPES and conducting research related to Interstellar Travel and Utilization of Nuclear Energy for Space Missions and Space Habitats. On the international front he is serving as the Advisory Council Member to United Nations Center for Space Science and Space Technology Education in Asia-Pacific Region (UN CSSTEAP) and he is also the Member of the Academic Council on United Nations Systems and Member of the European Association for International Education (EAIE).

He is also currently the member of NAFSA as an educator. Dr Ugur GUVEN has 25+ years of work experience and over 150+ academic publications comprising of journal papers, conference proceedings, project reports, and books.

Dr. Prakash S Kulkarni is an Aerospace Engineer with M.Tech and PhD from Indian Institute of Science. He currently works as Chief Research Scientist and Professor at Department of Aerospace Engineering, Indian Institute of Science, Bengaluru. He was involved in the development of various robust kinetic theory-based algorithms to include higher accuracy and high-fidelity physics to simulate complex flows and algorithms based on moving mesh for unsteady aerodynamics. Currently he works in applying these algorithms to the practical configurations for aerodynamic analysis, verification and validation. His other areas of interests include CFD for biofluids, flow control devices and parallel computing

Dr. Om Prakash is an Aerospace Engineer (PhD, B. E) and an expert in flight mechanics (M.Tech). He currently is working as Professor of Aerospace Engineering at UPES and conducting research in the areas of flight mechanics, modeling and simulation, parachute and parafoil systems. Dr. Om Prakash serves as Faculty and Head of Aerospace Engineering at UPES and he also held the position of Head of Department of Aerospace Engineering at BBD University, Lucknow.

Mr. Ganesh Pawar R is a Research Intern in Computational Mechanics Lab (CML), Dept., of Aerospace Engineering, IISc, Bengaluru. He has pursued his Master of Technology in Thermal Engineering and bachelor's degree in Mechanical Engineering from Visvesvaraya Technological University (VTU), Belagavi. His area of interest involves CFD algorithm development, Assessment of generalized finite difference method (Meshless method), and high speed internal and external flows. He holds, three research publications together in journal and national conference.